Inorganic Chemistry
Cite This: Inorg. Chem. 2019, 58, 15008−15012
Communication
pubs.acs.org/IC

Ligand-Dependent Luminescence Properties of Lanthanide−Titanium Oxo Clusters

Rong Chen,[†,§] Zi-Feng Hong,[†,§] Ya-Rui Zhao,[†] Hao Zheng,[†] Guan-Jun Li,[†] Qian-Chong Zhang,[‡] Xiang-Jian Kong,*[,†] La-Sheng Long,[†] and Lan-Sun Zheng[†]

[†]Collaborative Innovation Center of Chemistry for Energy Materials, State Key Laboratory of Physical Chemistry of Solid Surfaces, and Department of Chemistry, College of Chemistry and Chemical Engineering, Xiamen University, Xiamen 361005, China

[‡]State Key Laboratory of Structural Chemistry, Fujian Institute of Research on the Structure of Matter, Chinese Academy of Sciences, Fuzhou, Fujian 350002, China

Supporting Information

ABSTRACT: A series of lanthanide−titanium oxo clusters (LnTOCs), Ln_2Ti_8-Ac, Ln_2Ti_8-*p*-Toluic, and Ln_2Ti_8-Anthra (Ln = Eu and Tb), were prepared based on acetic acid (HAc), *p*-toluic acid (Hp-Toluic), and anthracene-9-carboxylic acid (HAnthra). Crystal structural analysis showed that these clusters possess the same metal topology framework, in which eight Ti^{4+} ions form a cube and two Ln^{3+} ions are located on the opposite faces of the cube. The luminescence investigation discovered that the Eu_2Ti_8−Ac displays the highest quantum yields with 15.6%, and the conjugation effect of ligand substituents can lower the triplet state energy of ligands, thus regulating the luminescence quantum yield of the Ln_2Ti_8 clusters. These results suggest that the triplet excited-state energy of the ligands should match well with the energy levels of Ln^{3+} to enhance the luminescence.

Lanthanide complexes have received more attention due to their interesting magnetic, electrical, optical, and catalytic properties and their potential applications in the fields of materials science, solar energy conversion, LED, biological imaging and sensing, and time-resolved immune testing.[1] Compared with the mononuclear lanthanide complexes, the polynuclear lanthanide clusters (4f),[2] especially the heterometallic lanthanide-transition (3d−4f) clusters,[3] exhibit special properties for the unique synergism between multiple metal ions in the cluster.[4] However, because of the quenching of many hydroxyl bridges and coordinated water molecules, most of the 4f/3d−4f clusters do not show high luminescence quantum yield (QY). Recent studies demonstrate that the lanthanide−titanium oxo clusters (LnTOC) generally have excellent luminescence performance not only because there are usually O-bridges instead of OH-bridges between metal ions and there is a decrease in water molecules but also because of the energy transfer between the lanthanide−titanium oxo core and the ligands.[5] Although lanthanide−titanium oxo cluster compounds have attracted extensive attention in the past few years, the synthesis of LnTOC is also a great challenge due to the very strong hydrolysis of Ti^{4+} ions. This difficulty in synthesis further prevents the systematic study of the luminescence properties of LnTOCs.

The intramolecular energy-transfer efficiency from the lowest triplet state of the ligand to the lowest excited state of Ln^{3+} ions plays an important role in the luminescence performance and the QY of a lanthanide complex.[6] The energy gap between the lowest triplet level of the ligand and the lowest excited level of the Ln^{3+} must be at an appropriate value for the high luminescence efficiency; for example, the triplet levels of ligands in the range of 22 000−27 000 cm^{-1} can effectively sensitize both Eu^{3+} and Tb^{3+} ions.[7,8] Different types of ligands have different triplet energy levels, so choosing appropriate ligands with a suitable triplet energy level is an ideal way to construct excellent luminescence performance.[7−9] There are a number of works that have been reported about the ligand dependence of the luminescence QY of Ln^{3+},[10] whereas works on the luminescence of LnTOCs are rare.

Herein, to investigate the energy transfer in the LnTOC system, we have chosen three carboxylic acid ligands with different substituents and prepared three series of heterometallic LnTOCs, formulated as $[Ln_2Ti_8(\mu_2\text{-}O)_2(\mu_3\text{-}O)_8(\mu_2\text{-}OH)_2(Ac)_{16}]\cdot 8(CH_3CN)$ (Ln_2Ti_8-Ac, Ln = Eu (1), Tb (2), HAc = acetic acid), $[Ln_2Ti_8(\mu_2\text{-}O)_2(\mu_3\text{-}O)_8(\mu_2\text{-}OH)_2(p\text{-toluic})_{16}]\cdot 2(H_2O)$ (Ln_2Ti_8-*p*-Toluic, Ln = Eu (3), Tb (4), Hp-Toluic = *p*-toluic acid), and $[Ln_2Ti_8(\mu_2\text{-}O)_2(\mu_3\text{-}O)_8(\mu_2\text{-}OH)_2(anthra)_{16}]\cdot 4((CH_3)_2CHOH)\cdot 12(H_2O)$ (Ln_2Ti_8-Anthra, Ln = Eu (5), Tb (6), HAnthra = anthracene-9-carboxylic acid). The luminescence investigation shows that the higher the electron-donating ability of the ligand substituent, the lower the triplet state (T_1) energies of the ligands. The Eu_2Ti_8−Ac displays the highest QY with 15.6% because of the appropriate T_1 level. The T_1 energies of Eu_2Ti_8-*p*-Toluic are very close to the excited level of Eu^{3+}, and the energy back transfer from Eu^{3+} to ligand was observed, which resulted in a 1.5% QY. Because the T_1 energies of Eu_2Ti_8-Anthra are lower than the excited level of Eu^{3+}, there is no energy transfer from the ligand to Eu^{3+} and no luminescence phenomenon. The Tb_2Ti_8 also shows similar luminescence properties.

Ln_2Ti_8-Ac, Ln_2Ti_8-*p*-Toluic, and Ln_2Ti_8-Anthra were prepared by the reaction of lanthanide salts, $Ti(O^iPr)_4$, and different ligands of acetic acid/*p*-toluic acid/anthracene-9-carboxylic acid in CH_3CN/IPA and THF. The single-crystal

Received: July 16, 2019
Published: November 5, 2019

DOI: 10.1021/acs.inorgchem.9b02112
Inorg. Chem. 2019, 58, 15008−15012

structural analysis shows that the Ln_2Ti_8-Ac clusters belong to the cubic crystal *Imm* space group; Ln_2Ti_8-*p*-Toluic and Ln_2Ti_8-Anthra crystallize in a tetragonal crystal *I*4/*m* and trigonal crystal *R*3*c* space group. These three series of Ln_2Ti_8 clusters have the same metal core as $[Ln_2Ti_8(\mu_2\text{-}O)_2(\mu_3\text{-}O)_8(\mu_2\text{-}OH)_2]^{16+}$. The metal core of $[Ln_2Ti_8(\mu_2\text{-}O)_2(\mu_3\text{-}O)_8(\mu_2\text{-}OH)_2]^{16+}$ is composed of two Ln^{3+} ions, eight Ti^{4+} ions, and two μ_2-O, eight μ_3-O^-, and two μ_2-OH bridges, as displayed in Figure 1a. The metal framework can be regarded

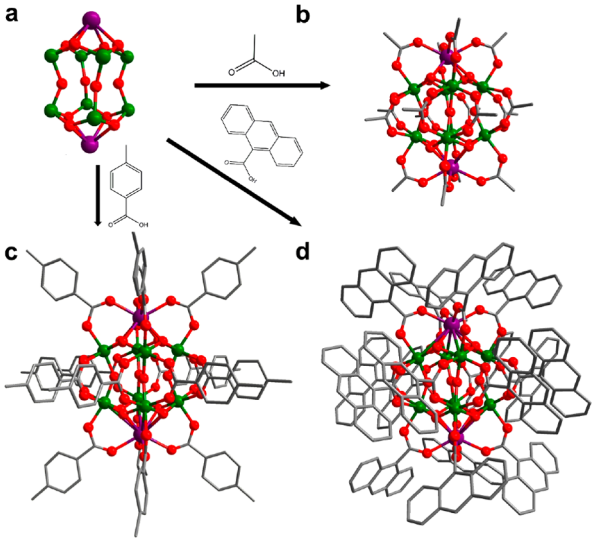

Figure 1. Crystal structures of (a) $[Ln_2Ti_8(\mu_2\text{-}O)_2(\mu_3\text{-}O)_8(\mu_2\text{-}OH)_2]^{16+}$, (b) Ln_2Ti_8-Ac, (c) Ln_2Ti_8-*p*-Toluic, and (d) Ln_2Ti_8-Anthra (Ln = Eu, Tb). Ln, purple; Ti, green; O, red; C, gray.

as a combination of two quadrangular pyramids linked by two μ_2-O bridges and two μ_2-OH bridges. As a result, the eight Ti^{4+} ions form a nearly cubic structure, and two Ln^{3+} ions locate on opposite faces of the cube (Figure S1). As shown in Figure 1b–d, the 10-metal core $[Ln_2Ti_8(\mu_2\text{-}O)_2(\mu_3\text{-}O)_8(\mu_2\text{-}OH)_2]^{16+}$ is further protected by 16 Ac^-, 16 *p*-toluic$^-$, and 16 anthra$^-$, generating the clusters of Ln_2Ti_8-Ac, Ln_2Ti_8-*p*-Toluic, and Ln_2Ti_8-Anthra, respectively. As shown in Figure S3, adjacent Ln_2Ti_8-Ac clusters are linked through hydrogen bonding, whereas adjacent Ln_2Ti_8-*p*-Toluic clusters are connected together by π–π stacking (Figure S4). Interestingly, a nanocage is formed by packing six Ln_2Ti_8-Anthra through π–π stacking and hydrogen bonding (Figure S5). Each Ln^{3+} displays an octa-tetragonal antiprism configuration and is coordinated by four μ_3-O atoms and four oxygen atoms from four protected ligands. All Ti^{4+} ions show a twisted octahedron and are six-coordinated by six oxygen atoms from two μ_3-O, one μ_2-O, and three ligands. The bond-length ranges of the Ti–O and Ln–O bonds are 1.803 to 2.085 and 2.328 to 2.581 Å, close to the distances reported in the literature.[5]

The images of the Eu_2Ti_8 and Tb_2Ti_8 crystal series under 365 nm irradiation are shown in Figure 2. Eu_2Ti_8-Ac and Eu_2Ti_8-*p*-Toluic display red emission, whereas Eu_2Ti_8-Anthra has no luminescence emission. For the Tb_2Ti_8 series, Tb_2Ti_8-Ac shows green emission, and the Tb_2Ti_8-*p*-Toluic shows faint green emission, whereas the Tb_2Ti_8-Anthra has no luminescence emission. These results clearly show the effect of different ligands on the luminescence properties. The emission and excitation spectra of the Eu_2Ti_8 and Tb_2Ti_8 series were measured at room temperature in the solid state and are shown

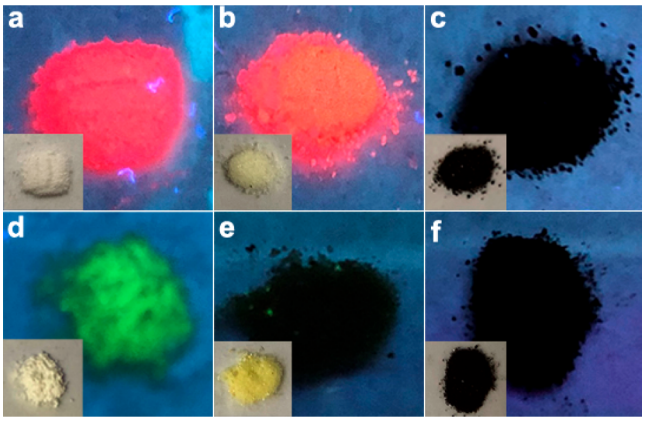

Figure 2. Images of (a) Eu_2Ti_8-Ac, (b) Eu_2Ti_8-*p*-Toluic, (c) Eu_2Ti_8-Anthra, (d) Tb_2Ti_8-Ac, (e) Tb_2Ti_8-*p*-Toluic, and (f) Tb_2Ti_8-Anthra under 365 nm irradiation. The insets are the corresponding images of the clusters under a daylight lamp.

in Figure 3 and Figures S9 and S10. Eu_2Ti_8-Ac clusters display the characteristic transitions of Eu(III) at 578 ($^5D_0 \rightarrow {}^7F_0$),

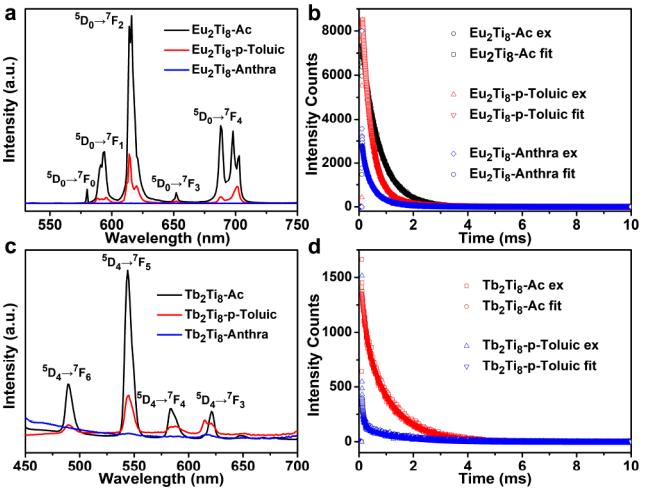

Figure 3. (a) Emission spectra and (b) lifetime of Eu_2Ti_8-Ac, Eu_2Ti_8-*p*-Toluic, and Eu_2Ti_8-Anthra. (c) Emission spectra and (d) lifetime of Tb_2Ti_8-Ac, Tb_2Ti_8-*p*-Toluic, and Tb_2Ti_8-Anthra.

592 ($^5D_0 \rightarrow {}^7F_1$), 615 ($^5D_0 \rightarrow {}^7F_2$), 652 ($^5D_0 \rightarrow {}^7F_3$), and 698 nm ($^5D_0 \rightarrow {}^7F_4$), respectively (Figure 3a).[11] The emission intensity of Eu_2Ti_8-*p*-Toluic obviously decreases, and almost no peaks of the Eu_2Ti_8-Anthra are observed. As shown in Figure 3b, the luminescence lifetimes (τ) of Eu_2Ti_8-Ac, Eu_2Ti_8-*p*-Toluic, and Eu_2Ti_8-Anthra are 6576, 1406, and 657 μs, respectively. The absolute QYs of Eu_2Ti_8-Ac and Eu_2Ti_8-*p*-Toluic are 15.6 and 1.5%. The τ and the absolute QY were both characterized at room temperature. The change trend of QYs is consistent with the luminescence intensity. In the Tb_2Ti_8 series, only Tb_2Ti_8-Ac exhibits the strong characteristic transitions of Tb(III) at 488 ($^5D_4 \rightarrow {}^7F_6$), 544 ($^5D_4 \rightarrow {}^7F_5$), 584 ($^5D_4 \rightarrow {}^7F_4$), and 620 ($^5D_4 \rightarrow {}^7F_3$) (Figure 3c).[12] The absolute QY of Tb_2Ti_8–Ac is 0.08%, and the lifetimes of Tb_2Ti_8–Ac and Tb_2Ti_8-*p*-Toluic are 1035 and 306 μs (Figure 3d).

To better understand the ligand effect on the luminescence performance, UV–vis absorption was measured to calculate the singlet state (S_1) energy of the ligand, and phosphor-

DOI: 10.1021/acs.inorgchem.9b02112
Inorg. Chem. 2019, 58, 15008–15012

escence was characterized to calculate the triplet state (T_1) energy of ligand. If the energy gap between S_1 and T_1 is larger than 5000 cm^{-1}, then the intersystem crossing (ISC) process will be more effective based on Reinhoudt's empirical rule.[12,13] As shown in Figures S11a, S12a, and S13, the UV−vis absorption peaks for HAc, Hp-Toluic, and HAnthra, are 210, 236, and 250 nm, corresponding to the $\pi-\pi$ transitions with the S_1 energy levels of 47 619, 42 373, and 40 000 cm^{-1}, respectively. The difference in energy levels was based on the conjugated extent of the ligands. The more conjugated bonds of the ligands would lead to a lower energy level. According to the phosphorescence of isostructural Gd_2Ti_8-HAc and Gd_2Ti_8-*p*-Toluic at room temperature (Figures S11b and S12b), HAc and *p*-toluic have triplet excited-state energies of 24 752 and 20 492 cm^{-1}. Therefore, the energy gaps between S_1 and T_1 of HAc and Hp-Toluic are 22 867 and 21 881 cm^{-1}, indicating that the ISC process is very efficient. However, the attempt to determine the T_1 energies of Gd_2Ti_8-Anthra failed because we did not obtain the crystal sample of Gd_2Ti_8-Anthra. The reported value of the triplet state energy for HAnthra was 14 900 cm^{-1} in the literature.[14]

The lowest T_1 energy of organic ligands must be higher than the resonance level of Ln^{3+} ions to play the role of an "antenna".[1a,10d,15] In general, the T_1 energy levels of ligands in the range of 22 000−27 000 cm^{-1} are the primary conditions for sensitizing both Eu^{3+} ($^5D_1$, 19 027 cm^{-1}) and Tb^{3+} ($^5D_4$, 20 500 cm^{-1}) to luminescence.[8b,13,14] The $^5D_1$ level will have a nonradiative decay process to the $^5D_0$ level of the Eu^{3+} ion, resulting in emission luminescence. As shown in Figure 4, the

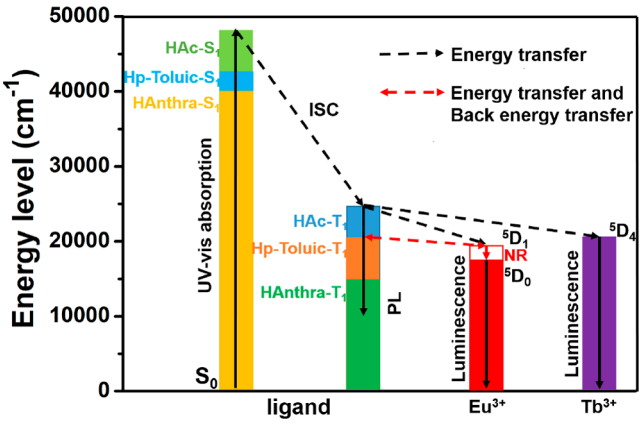

Figure 4. Schematic diagram of the energy transfer from the ligand to Eu^{3+}/Tb^{3+} in PL emission. The value of HAnthra-T_1 was reported in the literature.[13] PL, phosphorescence; ISC, intersystem crossing; NR, nonradiative decay.

T_1 (24 752 cm^{-1}) of HAc is suitable for the emission level of the Eu^{3+} ion, and the energy transfer from T_1 of Ac^- to $^5D_1$ of the Eu^{3+} ion is efficient. For Hp-Toluic, the T_1 (20 492 cm^{-1}) is close to the $^5D_1$ of the Eu^{3+} ion, and the energy can back-transfer from $^5D_1$ to T_1 of the Hp-Toluic ligand, resulting in the reduced luminescence QY. However, further conjugation decreases the T_1 energies and leads to the T_1 level of HAnthra being lower than the $^5D_1$ level of Eu^{3+}, so the HAnthra ligand cannot sensitize Eu^{3+}, and no luminescence emission of Eu^{3+} was observed.[16] For the Tb_2Ti_8 series, only the Ac^- can sensitize terbium, and the obvious green emission luminescence is observed. The lowest T_1 energies of Hp-Toluic are very close to the $^5D_4$ level of Tb^{3+}, resulting in a faint emission, whereas the lowest T_1 energies of HAnthra ligand are lower than the $^5D_4$ level of Tb^{3+}, leading to no emission for Tb_2Ti_8-Anthra.

In summary, we have reported two series of lanthanide−titanium oxo clusters Eu_2Ti_8 and Tb_2Ti_8 based on three carboxylic acid ligands with different substituents. The luminescence investigation shows that the acetate-based Eu_2Ti_8−Ac displays the highest QY of 15.6% because of the energy matching of the triplet state level of the acetate ligand with excited states $^5D_1$ of the Eu^{3+} ion. The conjugation effect of substituents can lower the triplet-state energy of the ligand and lead to reverse energy transfer from Ln^{3+} to the ligand, resulting in a decrease in the luminescence QY. This work demonstrates that ligand regulation can effectively improve the luminescence performance, which provides a reference for designing lanthanide luminescent materials with high performance.

■ ASSOCIATED CONTENT

Supporting Information

The Supporting Information is available free of charge on the ACS Publications website at DOI: 10.1021/acs.inorgchem.9b02112.

Experimental section, Tables S1−S9, and Figures S1−S13 (PDF)

Accession Codes

CCDC 1937671−1937676 contain the supplementary crystallographic data for this paper. These data can be obtained free of charge via www.ccdc.cam.ac.uk/data_request/cif, or by emailing data_request@ccdc.cam.ac.uk, or by contacting The Cambridge Crystallographic Data Centre, 12 Union Road, Cambridge CB2 1EZ, UK; fax: +44 1223 336033.

■ AUTHOR INFORMATION

Corresponding Author

*E-mail: xjkong@xmu.edu.cn.

ORCID

Qian-Chong Zhang: 0000-0001-9701-0106

Xiang-Jian Kong: 0000-0003-0676-6923

La-Sheng Long: 0000-0002-0398-4709

Author Contributions

§R.C. and Z.-F.H. contributed equally.

Notes

The authors declare no competing financial interest.

■ ACKNOWLEDGMENTS

This work was supported by the National Natural Science Foundation of China (grants nos. 21871224, 21673184, 21431005, and 21721001) and the Fundamental Research Funds for the Central Universities (20720180032).

■ REFERENCES

(1) (a) Moore, E. G.; Samuel, A. P. S.; Raymond, K. N. From Antenna to Assay: Lessons Learned in Lanthanide Luminescence. *Acc. Chem. Res.* **2009**, *42*, 542−552. (b) Shinoda, S.; Tsukube, H. Luminescent lanthanide complexes as analytical tools in anion sensing, pH indication and protein recognition. *Analyst* **2011**, *136*, 431−435. (c) Duke, R. M.; Veale, E. B.; Pfeffer, F. M.; Kruger, P. E.; Gunnlaugsson, T. Colorimetric and fluorescent anion sensors: an overview of recent developments in the use of 1,8-naphthalimide-based chemosensors. *Chem. Soc. Rev.* **2010**, *39*, 3936−3953. (d) Tsukube, H.; Shinoda, S. Lanthanide Complexes in Molecular

DOI: 10.1021/acs.inorgchem.9b02112
Inorg. Chem. 2019, 58, 15008−15012

Recognition and Chirality Sensing of Biological Substrates. *Chem. Rev.* **2002**, *102*, 2389−2404. (e) Pan, M.; Liao, W.-M.; Yin, S.-Y.; Sun, S.-S.; Su, C.-Y. Single-Phase White-Light-Emitting and Photoluminescent Color-Tuning Coordination Assemblies. *Chem. Rev.* **2018**, *118*, 8889−8935.

(2) (a) Fernandez Garcia, G.; Guettas, D.; Montigaud, V.; Larini, P.; Sessoli, R.; Totti, F.; Cador, O.; Pilet, G.; Le Guennic, B. A. Dy_4Cubane: A New Member in the Single-Molecule Toroics Family. *Angew. Chem., Int. Ed.* **2018**, *57*, 17089−17093. (b) Li, X.-Y.; Su, H.-F.; Li, Q.-W.; Feng, R.; Bai, H.-Y.; Chen, H.-Y.; Xu, J.; Bu, X.-H. A Giant Dy_{76} Cluster: A Fused Bi-Nanopillar Structural Model for Lanthanide Clusters. *Angew. Chem., Int. Ed.* **2019**, *58*, 10184−10188. (c) Zheng, Z.-P. Ligand-controlled self-assembly of polynuclearlanthanide-oxo/hydroxo complexes: from synthetic serendipity to rational supramolecular design. *Chem. Commun.* **2001**, 2521−2529. (d) Liu, J.-L.; Chen, Y.-C.; Tong, M.-L. Symmetry strategies for high performance lanthanide-based single-molecule magnets. *Chem. Soc. Rev.* **2018**, *47*, 2431−2453. (e) Peng, J.-B.; Kong, X.-J.; Zhang, Q.-C.; Orendáč, M.; Prokleška, J.; Ren, Y.-P.; Long, L.-S.; Zheng, Z.-P.; Zheng, L.-S. Beauty, Symmetry, and Magnetocaloric Effect-Four-Shell Keplerates with 104 Lanthanide Atoms. *J. Am. Chem. Soc.* **2014**, *136*, 17938−17941. (f) Zheng, X.-Y.; Jiang, Y.-H.; Zhuang, G.-L.; Liu, D.-P.; Liao, H.-G.; Kong, X.-J.; Long, L.-S.; Zheng, L.-S. A Gigantic Molecular Wheel of $\{Gd_{140}\}$: A New Member of the Molecular Wheel Family. *J. Am. Chem. Soc.* **2017**, *139*, 18178−18181. (g) Wu, M.-Y.; Jiang, F.-L.; Kong, X.-J.; Yuan, D.-Q.; Long, L.-S.; Al-Thabaiti, S. A.; Hong, M.-C. Two polymeric 36-metal pure lanthanide nanosizeclusters. *Chem. Sci.* **2013**, *4*, 3104−3109. (h) Dong, J.; Cui, P.; Shi, P. F.; Cheng, P.; Zhao, B. Ultrastrong Alkali-Resisting Lanthanide-Zeolites Assembled by $[Ln_{60}]$ Nanocages. *J. Am. Chem. Soc.* **2015**, *137*, 15988−15991.

(3) (a) Fang, W.-H.; Yang, G.-Y. Induced Aggregation and Synergistic Coordination Strategy in Cluster Organic Architectures. *Acc. Chem. Res.* **2018**, *51*, 2888−2896. (b) Baniodeh, A.; Liang, Y.; Anson, C. E.; Magnani, N.; Powell, A. K.; Unterreiner, A.-N.; Seyfferle, S.; Slota, M.; Dressel, M.; Bogani, L.; Goß, K. Unraveling the Influence of Lanthanide Ions on Intra- and Inter-Molecular Electronic Processes in $Fe_{10}Ln_{10}$ Nano-Toruses. *Adv. Funct. Mater.* **2014**, *24*, 6280−6290. (c) Chen, W.-P.; Liao, P.-Q.; Yu, Y.-Z.; Zheng, Z.-P.; Chen, X.-M.; Zheng, Y.-Z. A Mixed-Ligand Approach for a Gigantic and Hollow Heterometallic Cage $\{Ni_{64}RE_{96}\}$ for Gas Separation and Magnetic Cooling Applications. *Angew. Chem., Int. Ed.* **2016**, *55*, 9375−9379. (d) Zheng, X.-Y.; Xie, J.; Kong, X.-J.; Long, L.-S.; Zheng, L.-S. Recent advances in the assembly of high-nuclearity lanthanide clusters. *Coord. Chem. Rev.* **2019**, *378*, 222−236. (e) Zheng, H.; Du, M.-H.; Lin, S.-C.; Tang, Z.-C.; Kong, X.-J.; Long, L.-S.; Zheng, L.-S. Assembly of a Wheel-Like $Eu_{24}Ti_8$ Cluster under the Guidance of High-Resolution Electrospray Ionization Mass Spectrometry. *Angew. Chem., Int. Ed.* **2018**, *57*, 10976−10979. (f) Zheng, X.-Y.; Zhang, H.; Wang, Z.; Liu, P.; Du, M.-H.; Han, Y.-Z.; Wei, R.-J.; Ouyang, Z.-W.; Kong, X.-J.; Zhuang, G.-L.; Long, L.-S.; Zheng, L.-S. Insights into Magnetic Interactions in a Monodisperse $Gd_{12}Fe_{14}$ Metal Cluster. *Angew. Chem., Int. Ed.* **2017**, *56*, 11475−11479. (g) Zhang, Z.-M.; Pan, L.-Y.; Lin, W.-Q.; Leng, J.-D.; Guo, F.-S.; Chen, Y.-C.; Liu, J.-L.; Tong, M.-L. Wheel-shaped nanoscale 3d−4f $\{Co^{II}_{16}Ln^{III}_{24}\}$ clusters (Ln = Dy and Gd). *Chem. Commun.* **2013**, *49*, 8081−8083. (h) Yang, X.; Wang, S.; Schipper, D.; Zhang, L.; Li, Z.; Huang, S.; Yuan, D.; Chen, Z.; Gnanam, A. J.; Hall, J. W.; King, T. L.; Que, E.; Dieye, Y.; Vadivelu, J.; Brown, K. A.; Jones, R. A. Self-assembly of high-nuclearity lanthanide-based nanoclusters for potential bioimaging applications. *Nanoscale* **2016**, *8*, 11123−11129.

(4) (a) Zheng, X.-Y.; Kong, X.-J.; Zheng, Z.-P.; Long, L.-S.; Zheng, L.-S. High-Nuclearity Lanthanide-Containing Clusters as Potential Molecular Magnetic Coolers. *Acc. Chem. Res.* **2018**, *51*, 517−525. (b) Chen, W.-P.; Singleton, J.; Qin, L.; Camon, A.; Engelhardt, L.; Luis, F.; Winpenny, R. E. P.; Zheng, Y.-Z. Quantum Monte Carlo simulations of a giant $\{Ni_{21}Gd_{20}\}$ cage with a S = 91 spin ground state. *Nat. Commun.* **2018**, *9*, 2107−2112. (c) Chen, R.; Yan, Z.-H.; Kong, X.-J.; Long, L.-S.; Zheng, L.-S. Integration of Lanthanide−Transition-Metal Clusters onto CdS Surfaces for Photocatalytic Hydrogen Evolution. *Angew. Chem., Int. Ed.* **2018**, *57*, 16796−16800. (d) Zhu, Z.; Guo, M.; Li, X.-L.; Tang, J. K. Molecular magnetism of lanthanide: Advances and perspectives. *Coord. Chem. Rev.* **2019**, *378*, 350−364.

(5) (a) Lv, Y.; Willkomm, J.; Leskes, M.; Steiner, A.; King, T. C.; Gan, L.; Reisner, E.; Wood, P. T.; Wright, D. S. Formation of $Ti_{28}Ln$ Cages, theHighest NuclearityPolyoxotitanates (Ln = La, Ce). *Chem. - Eur. J.* **2012**, *18*, 11867−11870. (b) Wang, S.; Su, H. C.; Yu, L.; Zhao, X. W.; Qian, L. W.; Zhu, Q. Y.; Dai, J. Fluorescence and energy transfer properties of heterometalliclanthanide-titanium oxo clusters coordinated with anthracenecarboxylateligands. *Dalton Trans.* **2015**, *44*, 1882−1888. (c) Lu, D.-F.; Hong, Z.-F.; Xie, J.; Kong, X.-J.; Long, L.-S.; Zheng, L.-S. High-Nuclearity Lanthanide−Titanium Oxo Clusters as Luminescent Molecular Thermometers with High Quantum Yields. *Inorg. Chem.* **2017**, *56*, 12186−12192. (d) Zhang, G. L.; Wang, S.; Hou, J. L.; Mo, C. J.; Que, C. J.; Zhu, Q. Y.; Dai, J. A lanthanide−titanium ($LnTi_{11}$) oxo-cluster, a potential molecule based fluorescent labelling agent and photocatalyst. *Dalton Trans.* **2016**, *45*, 17681−17686. (e) Lu, D.-F.; Kong, X.-J.; Lu, T.-B.; Long, L.-S.; Zheng, L.-S. Heterometallic Lanthanide−Titanium Oxo Clusters: A New Family of Water Oxidation Catalysts. *Inorg. Chem.* **2017**, *56*, 1057−1060.

(6) D'Aléo, A.; Pointillart, F.; Ouahab, L.; Andraud, C.; Maury, O. Charge transfer excited states sensitization of lanthanide emitting from the visible to the near-infra-red. *Coord. Chem. Rev.* **2012**, *256*, 1604−1620.

(7) de Sá, G. F.; Malta, O. L.; de Mello Donegá, C.; Simas, A. M.; Longo, R. L.; Santa-Cruz, P. A.; da Silva, E. F. Spectroscopic properties and design of highly luminescent lanthanide coordination complexes. *Coord. Chem. Rev.* **2000**, *196*, 165−195.

(8) (a) Cui, Y.-J.; Yue, Y.-F.; Qian, G.-D.; Chen, B.-L. Luminescent Functional Metal−Organic Frameworks. *Chem. Rev.* **2012**, *112*, 1126−1162. (b) Latva, M.; Takalo, H.; Mukkala, V.-M.; Matachescu, C.; Rodríguez-Ubis, J. C.; Kankare, J. Correlation between the lowest triplet state energy level of the ligand and lanthanide(III) luminescence quantum yield. *J. Lumin.* **1997**, *75*, 149−169.

(9) (a) Varaksina, E. A.; Taydakov, V.; Ambrozevich, S. A.; Selyukov, A. S.; Lyssenko, K. A.; Jesus, L. T.; Freire, R. O. Influence of fluorinated chain length on luminescent properties of Eu^{3+} β-diketonate complexes. *J. Lumin.* **2018**, *196*, 161−168. (b) Pan, M.; Du, B.-B.; Zhu, Y.-X.; Yue, M.-Q.; Wei, Z.-W.; Su, C.-Y. Highly Efficient Visible-to-NIR Luminescence of Lanthanide(III) Complexes with Zwitterionic Ligands Bearing Charge-Transfer Character: Beyond Triplet Sensitization. *Chem. - Eur. J.* **2016**, *22*, 2440−2451. (c) Pan, M.; Zhu, Y.-X.; Wu, K.; Chen, L.; Hou, Y.-J.; Yin, S.-Y.; Wang, H.-P.; Fan, Y.-N.; Su, C.-Y. Epitaxial Growth of Hetero-Ln-MOF Hierarchical Single Crystals for Domain- and Orientation-Controlled Multicolor Luminescence 3D Coding Capability. *Angew. Chem., Int. Ed.* **2017**, *56*, 14582−14586.

(10) (a) Bettencourt-Dias, A. Small Molecule Luminescent Lanthanide Ion Complexes-Photophysical Characterization and Recent Developments. *Curr. Org. Chem.* **2007**, *11*, 1460−1480. (b) Di Pietro, S. Di; Gautier, N.; Imbert, D.; Pécaut, J.; Mazzanti, M. Versatile pyridine-2,6-bis-tetrazolate scaffolds for the formation of highly luminescent lanthanide complexes. *Dalton Trans.* **2016**, *45*, 3429−3442. (c) Matthes, P. R.; Nitsch, J.; Kuzmanoski, A.; Feldmann, C.; Steffen, A.; Marder, T. B.; Müller-Buschbaum, K. The Series of Rare Earth Complexes $[Ln_2Cl_6(\mu\text{-}4,4'\text{-bipy})(py)_6]$, Ln = Y, Pr, Nd, Sm-Yb: A Molecular Model System for Luminescence Properties in MOFs Based on $LnCl_3$ and 4,4′-Bipyridine. *Chem. - Eur. J.* **2013**, *19*, 17369−17378. (d) Bünzli, J.-C. G. Lanthanide Luminescence for Biomedical Analyses and Imaging. *Chem. Rev.* **2010**, *110*, 2729−2755.

(11) Thielemann, D. T.; Wagner, A. T.; Rösch, E.; Kölmel, D. K.; Heck, J. G.; Rudat, B.; Neumaier, M.; Feldmann, C.; Schepers, U.; Bräse, S.; Roesky, P. W. Luminescent Cell-Penetrating Pentadecanuclear Lanthanide Clusters. *J. Am. Chem. Soc.* **2013**, *135*, 7454−7457.

DOI: 10.1021/acs.inorgchem.9b02112
Inorg. Chem. 2019, 58, 15008−15012

(12) Lewis, D. J.; Glover, P. B.; Solomons, M. C.; Pikramenou, Z. Purely Heterometallic Lanthanide(III) Macrocycles through Controlled Assembly of Disulfide Bonds for Dual Color Emission. *J. Am. Chem. Soc.* **2011**, *133*, 1033−1043.
(13) Zhou, J.-M; Li, H.-H.; Zhang, H.; Li, H.-M.; Shi, W.; Cheng, P. A Bimetallic Lanthanide Metal−Organic Material as a Self-Calibrating Color-Gradient Luminescent Sensor. *Adv. Mater.* **2015**, *27*, 7072−7077.
(14) Parker, D. Luminescent lanthanide sensors for pH, pO2 and selected anions. *Coord. Chem. Rev.* **2000**, *205*, 109−130.
(15) (a) Binnemans, K. Lanthanide-Based Luminescent Hybrid Materials. *Chem. Rev.* **2009**, *109*, 4283−4374. (b) Crosby, G. A.; Whan, R. E.; Alire, R. M. Intramolecular Energy Transfer in Rare Earth Chelates. Role of the Triplet State. *J. Chem. Phys.* **1961**, *34*, 743−748.
(16) Hilder, M.; Junk, P. C.; Kynast, U. H.; Lezhnina, M. M. Spectroscopic properties of lanthanoid benzene carboxylates in the solid state: Part 1. *J. Photochem. Photobiol., A* **2009**, *202*, 10−20.

DOI: 10.1021/acs.inorgchem.9b02112
Inorg. Chem. 2019, 58, 15008−15012